Superfluid vortex dynamics on an ellipsoid and other surfaces of revolution

Mônica A. Caracanhas [1], Pietro Massignan [2,*] and Alexander L. Fetter [3,†]
[1]*Instituto de Física de São Carlos, Universidade de São Paulo, São Paulo 13566-590, Brazil*
[2]*Departament de Física, Universitat Politècnica de Catalunya, Campus Nord B4-B5, E-08034 Barcelona, Spain*
[3]*Departments of Physics and Applied Physics, Stanford University, Stanford, California 94305, USA*

(Received 29 October 2021; accepted 10 January 2022; published 7 February 2022)

We present a study of superfluid vortex dynamics on general axisymmetric compact surfaces with no holes. Specifically, we develop a general method to transform conformally from the axisymmetric surface to a plane, where we use familiar methods based on the hydrodynamic stream function. Our approach shows that vortices constitute a Hamiltonian dynamical system, with their angular positions on the surface as canonical variables. The dynamical motion conserves both the total energy and the angular momentum, and it features a marked anticorrelation between the vortex speed and the local curvature of the surface.

DOI: 10.1103/PhysRevA.105.023307

I. INTRODUCTION

Quantized vortices play an essential role in the physics of superfluids, such as ^{4}He-II [1], Bose-Einstein condensates (BECs), and fermionic superfluids of ultracold dilute atomic gases [2,3]. The dynamics of quantized vortices simplifies considerably for thin films where vortex-line bending is absent. At low temperature, these superfluids are effectively ideal fluids with no dissipation and obey equations of classical hydrodynamics [4,5], along with the condition of quantized vorticity [6,7].

Most studies have focused on planar superfluid films, but Lamb remarks in Sec. 160 of Ref. [5] that the theory can be generalized to curved surfaces and quotes some results for a spherical film. He relies on the method of stereographic projection, which maps the surface of a sphere to the complex plane where the familiar formalism of vortex hydrodynamics works well. A recent work by two of us [8] provides more details on this approach on a sphere along with many other references. Other simple conformal transformations permit studying the dynamics on surfaces with zero Gaussian curvature, such as cylinders and cones [9–11].

Many theoretical papers have explored the properties of a BEC trapped in a spherically symmetric shell potential [8,12–16], but recent experimental advances raise the important new question of vortex dynamics on more general surfaces of revolution. For example, Sachkou *et al.* reported studies of superfluid vortices generated over suspended microtoroidal optical resonators coated with He-II films [17]. Moreover, shell potentials for ultracold atoms have been generated by superposing quadrupolar and oscillatory magnetic fields [18–20]. The resulting spatially dependent dressed atomic states experience an effective axisymmetric ellipsoidal potential.

Experiments performed in the NASA Cold Atom Laboratory aboard the International Space Station recently produced three-dimensional BECs with no gravity [21], providing a more realistic possibility to explore bubble trapped BECs [22]. One of the aims of these experiments is the generation of vortices, which can be achieved by rotating the dressed trap or through the spontaneous creation of vortex-antivortex pairs across the condensation transition, namely, through the Kibble-Zurek mechanism [22–24].

In contrast to the spherical case, however, finding a conformal projection of an ellipsoidal surface to the flat plane is a complicated task. To solve this problem, we rely on the method of isothermal coordinates, inspired by Kirchhoff's early study of the surface of a torus [4,25,26]. Briefly, one seeks a coordinate transformation of the relevant surface metric to make it resemble the metric on the complex plane. For a sphere, this method immediately reproduces the result of stereographic projection, but it applies much more widely. Section II uses this metric method for quite general axisymmetric compact surfaces, and we illustrate it with the complex potential for a vortex dipole on one such surface, including the phase pattern and streamlines. Reference [27] anticipated several of our results in more formal mathematical language. See also Refs. [28–30] for other related material. Section III then studies vortex dynamics on such a general axisymmetric surface. Similar to the situation on a plane, these dynamical equations assume a Hamiltonian form with the coordinates of each vortex serving as a pair of canonical variables and the total energy serving as the Hamiltonian. One new feature is the appearance of local curvature contributions to the energy [26,31] that play an essential role in the vortex dynamics. In Sec. IV we apply this general formalism to an ellipsoid of revolution. Section V studies the dynamics of a vortex dipole for two highly symmetric initial configurations on an axisymmetric ellipsoid, along with a more general asymmetric configuration. We end with conclusions and discussion in Sec. VI.

*pietro.massignan@upc.edu
†fetter@stanford.edu

II. AXISYMMETRIC COMPACT SURFACES

The surface of a sphere of radius a satisfies the familiar set of equations

$$x = a\sin\theta\cos\phi, \quad y = a\sin\theta\sin\phi, \quad z = a\cos\theta, \tag{1}$$

where (θ, ϕ) are the usual spherical polar coordinates, with $0 < \theta < \pi$ measured from the north pole and $0 < \phi < 2\pi$ measured from the x axis.

More generally, the surface of an ellipsoid of revolution has the corresponding set of equations

$$x = a\sin\theta\cos\phi, \quad y = a\sin\theta\sin\phi, \quad z = b\cos\theta, \tag{2}$$

where a is the radius in the xy plane and b is the radius along the symmetry axis. In particular, this surface obeys the expected equation

$$\frac{x^2+y^2}{a^2} + \frac{z^2}{b^2} = 1. \tag{3}$$

Note that θ is now merely an abstract parameter defining the coordinates of the ellipsoidal surface. Its relation to the usual polar angle of spherical coordinates, and more generally to the so-called geocentric coordinates, requires a separate discussion (see Sec. IV).

Although we shall specialize to an axisymmetric ellipsoid, the formalism developed below applies widely, and we have found it helpful to consider a general compact surface of revolution described by the set of equations (compare Refs. [26,27])

$$x = f_1(\theta)\cos\phi, \quad y = f_1(\theta)\sin\phi, \quad z = f_2(\theta), \tag{4}$$

where, as in Eq. (2) above, f_1 and f_2 have the dimension of a length. We require $f_1(\theta) > 0$ to avoid self-intersection, $f_1(0) = f_1(\pi) = 0$ for a closed surface, and $f_2(0) > 0 > f_2(\pi)$ in analogy with the spherical case.

It is straightforward to find the metric for the surface defined in Eq. (4):

$$ds^2 = [f_1'(\theta)^2 + f_2'(\theta)^2]d\theta^2 + f_1(\theta)^2 d\phi^2 \equiv h_\theta^2 d\theta^2 + h_\phi^2 d\phi^2, \tag{5}$$

where we define the metric parameters

$$h_\theta = \sqrt{f_1'(\theta)^2 + f_2'(\theta)^2}, \quad h_\phi = f_1(\theta). \tag{6}$$

The presence of two different parameters h_θ and h_ϕ in Eq. (5) precludes a simple description with a single complex variable involving θ and ϕ directly.

The standard procedure is to seek a coordinate transformation from Eq. (5) to new "isothermal" variables (u, v), defined as having an isotropic metric $ds^2 = \lambda^2(du^2 + dv^2)$ with an overall scale factor λ. For the present paper, we prefer the polar form $u + iv = \rho\, e^{i\phi}$, with $\rho^2 = u^2 + v^2$, $\tan\phi = v/u$, and

$$ds^2 = \lambda^2(d\rho^2 + \rho^2 d\phi^2). \tag{7}$$

Focus on the common azimuthal angle ϕ and write Eq. (5) as

$$ds^2 = h_\phi^2\left(\frac{h_\theta^2}{h_\phi^2}d\theta^2 + d\phi^2\right). \tag{8}$$

We now compare this metric to Eq. (7) for a plane rewritten in the form

$$ds^2 = \lambda^2\rho^2\left(\frac{d\rho^2}{\rho^2} + d\phi^2\right). \tag{9}$$

Evidently, we should require

$$\frac{d\rho}{\rho} = \frac{h_\theta}{h_\phi}d\theta, \tag{10}$$

which can be integrated to give

$$\ln\rho(\theta) = \int^\theta d\tilde\theta\,\frac{h_\theta}{h_\phi} = \int^\theta d\tilde\theta\,\frac{\sqrt{f_1'(\tilde\theta)^2 + f_2'(\tilde\theta)^2}}{f_1(\tilde\theta)}, \tag{11}$$

apart from an additive constant that will be irrelevant because of overall vortex-charge neutrality for a compact surface. As a result, the transformed metric has the desired isothermal form in Eq. (7) with overall scale factor

$$\lambda(\theta) = \frac{h_\phi(\theta)}{\rho(\theta)}. \tag{12}$$

III. VORTEX DYNAMICS ON AN AXISYMMETRIC COMPACT SURFACE

Throughout this whole paper we will be dealing with an incompressible superfluid covering a curved two-dimensional surface (embedded in three-dimensional space), and with isotropic (contact s-wave) interactions between the particles. The fluid has therefore a uniform thickness and a uniform density, and its coherence length ξ is much smaller than other relevant length scales in the problem. As a result, all quantum vortices in the fluid can be thought of being "pointlike" and having a common radius ξ_0, which remains at all times constant over the surface. A fluid is termed *ideal* when it is both irrotational and incompressible, i.e., when its velocity field $\boldsymbol{v}$ obeys $\boldsymbol{\nabla}\times\boldsymbol{v} = 0$ and $\boldsymbol{\nabla}\cdot\boldsymbol{v} = 0$. Remarkably, ultracold dilute superfluid quantum gases (in the Thomas-Fermi regime) and low-temperature superfluid ^{4}He both act like ideal fluids, facilitating the study of these important mathematical models. These quantum superfluids have a complex order parameter $\Psi = |\Psi|e^{i\Phi}$ with magnitude $|\Psi|$ and phase Φ. For such one-component quantum systems, the gradient of the phase determines the flow velocity [7]:

$$\boldsymbol{v} = \frac{\hbar}{M}\boldsymbol{\nabla}\Phi, \tag{13}$$

where $2\pi\hbar$ is Planck's constant and M is the relevant atomic mass. Equation (13) ensures that the flow velocity is irrotational; more unusually, it also implies that the circulation $\kappa = \oint_{\mathcal{C}} d\boldsymbol{l}\cdot\boldsymbol{v} = q\,2\pi\hbar/M$ along any closed path $\mathcal{C}$ is quantized in units of $2\pi\hbar/M$, where q is an integer. In most cases, quantized vortices are singly quantized, with unit vortex charge $q = \pm 1$.

In addition to the representation of $\boldsymbol{v}$ in terms of the quantum velocity potential $\Phi(x, y)$, the condition of incompressibility allows a different representation of $\boldsymbol{v}$ in terms of a vector potential $\boldsymbol{A}$, with $\boldsymbol{v} = \boldsymbol{\nabla}\times\boldsymbol{A}$. For a uniform two-dimensional fluid on a plane, this condition simplifies to

$$\boldsymbol{v} = \frac{\hbar}{M}\hat{\boldsymbol{n}}\times\boldsymbol{\nabla}\chi, \tag{14}$$

where $\chi(x, y)$ is the stream function and $\hat{\boldsymbol{n}} = \hat{\boldsymbol{x}} \times \hat{\boldsymbol{y}}$ is the unit normal vector.

Although both representations of $\boldsymbol{v}$ are important, the stream function χ offers a significant advantage here because of the quantized circulation mentioned above. Specifically, the vorticity $\boldsymbol{\zeta} = \boldsymbol{\nabla} \times \boldsymbol{v}$ for a positive singly charged vortex at the origin is singular with $\boldsymbol{\zeta}(\boldsymbol{r}) = (2\pi\hbar/M)\hat{\boldsymbol{n}}\,\delta^{(2)}(\boldsymbol{r})$. As a result, the corresponding stream function obeys the scalar Poisson equation $\nabla^2\chi = 2\pi\delta^{(2)}(\boldsymbol{r})$. It is clear that the stream function itself is effectively a two-dimensional Green's function, analogous to the more familiar electrostatic potential for a point charge in three dimensions. Our conformal transformation provides a powerful technique for constructing the Green's function on an axisymmetric curved surface.

Equations (13) and (14) each express the velocity components v_x and v_y as derivatives of the scalar functions χ and Φ. In detail, these equations are the Cauchy-Riemann equations for the complex potential

$$F(z) = \chi(\boldsymbol{r}) + i\,\Phi(\boldsymbol{r}) \tag{15}$$

that depends only on the single complex variable $z = x + iy$. In addition, the derivative of the complex potential determines the hydrodynamic flow velocity through the important relation

$$v_y + iv_x = \frac{\hbar}{M}\frac{dF}{dz} = \frac{\hbar}{M}F'(z). \tag{16}$$

On the complex plane, the familiar formalism gives the complex potential

$$F_0(z) = q_0 \ln(z - z_0) \tag{17}$$

for a single vortex with charge q_0 at z_0. Correspondingly, the complex hydrodynamic velocity field is

$$v_y + iv_x = \frac{\hbar q_0}{M(z - z_0)} \tag{18}$$

representing circular flow centered at z_0.

On a plane, a closed curve $\mathcal{C}$ defines an inside and an outside. The circulation integral along the contour $\mathcal{C}$ surrounding the interior region characterizes the enclosed vorticity, which must be an integer multiple of $2\pi\hbar/M$ for a superfluid. This result follows because Eq. (13) ensures that the line integral is essentially the net change in Φ around $\mathcal{C}$. Each vortex has lines of constant phase emerging from or ending at its location, just like the lines of electric field around point charges in two dimensions. On a plane, these lines of constant phase can extend to infinity.

The situation is very different for a compact surface like that introduced in Sec. II. Here, a closed curve merely divides the surface into two regions. For the first region, the line integral $\oint_{\mathcal{C}} d\boldsymbol{l} \cdot \boldsymbol{v}$ still equals an integral multiple of $2\pi\hbar/M$, but the corresponding lines of constant phase must reconverge somewhere on the compact surface. Specifically, consider the other region, where the contour integral $\oint_{\mathcal{C}} d\boldsymbol{l} \cdot \boldsymbol{v}$ now has an opposite orientation, yielding a circulation equal and opposite to the one in the first region. As a result, the total vortex charge on any compact surface must vanish, with a vortex dipole as the simplest such configuration.

For a plane, Eq. (17) shows that the complex potential for a vortex dipole is the difference of two logarithms $F_{\text{dipole}}(z) = \ln(z - z_+) - \ln(z - z_-) = \ln[(z - z_+)/(z - z_-)]$. The previous coordinate transformation now gives the desired expression for a vortex dipole on a quite general axisymmetric compact surface:

$$F_{\text{dipole}} = \ln\left(\frac{\rho\, e^{i\phi} - \rho_+\, e^{i\phi_+}}{\rho\, e^{i\phi} - \rho_-\, e^{i\phi_-}}\right) \tag{19}$$

in an obvious short-hand notation. This complex function gives all necessary information about the hydrodynamic flow field on the surface. For example, lines of constant phase $\Phi_{\text{dipole}} = \text{Im}\, F_{\text{dipole}}$ emerge from the positive vortex and end on the negative vortex. In addition, lines of constant stream function

$$\begin{aligned}\chi_{\text{dipole}} &= \text{Re}\, F_{\text{dipole}} \\ &= \frac{1}{2}\ln\left[\frac{\rho^2 - 2\rho\rho_+\cos(\phi - \phi_+) + \rho_+^2}{\rho^2 - 2\rho\rho_-\cos(\phi - \phi_-) + \rho_-^2}\right]\end{aligned} \tag{20}$$

trace out the lines of particle flow. Figure 1 shows the phase pattern and streamlines for one compact surface that

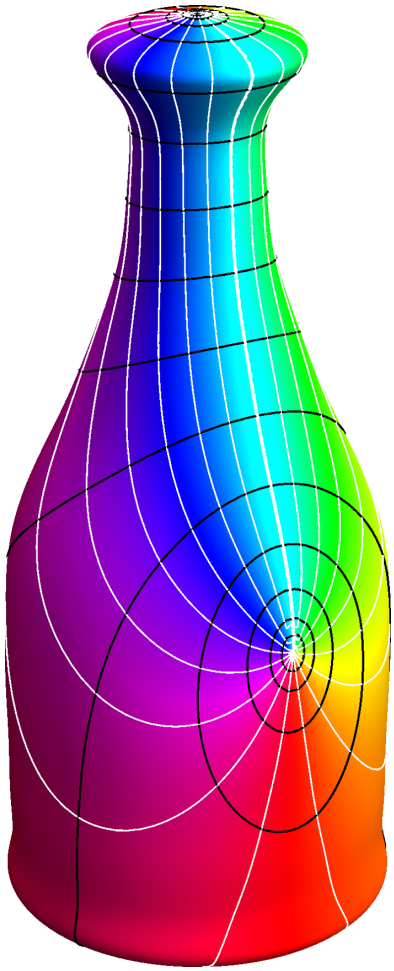

FIG. 1. Color wheel showing the phase pattern generated by a vortex dipole on a superfluid film covering a surface of revolution akin to a champagne bottle. White lines are lines of constant phase and black lines are stream lines. In the configuration displayed, one vortex is at the north pole and the other is on the side.

resembles a champagne bottle, where the function $\rho(\theta)$ was evaluated numerically.

On a planar surface, each member of a vortex dipole moves with the local velocity after subtracting the local circulating velocity of the particular vortex in question. But the transformation from the curved surface to the complex plane introduces an additional contribution. On the physical surface of the object, all point vortices have the same core size ξ_0 that serves to regularize the singularity at its center. On the complex plane, however, the scale factor λ renormalizes each vortex core size to $\xi_j = \xi_0/\lambda_j$, where λ_j denotes the scale factor evaluated at the position of the jth vortex. See Sec. VI of Ref. [31] for a more detailed discussion of this important issue.

The numerator of Eq. (20) provides the flow arising from the positive vortex. It contains the combination $\rho^2 - 2\rho\rho_+\cos(\phi-\phi_+) + \rho_+^2$, which can be rewritten exactly as $(\rho-\rho_+)^2 + 4\rho\rho_+\sin^2[(\phi-\phi_+)/2]$. For small $d\theta = \theta - \theta_+$ and $d\phi = \phi - \phi_+$, this quantity reduces to $(\rho_+^2/h_{\phi_+}^2)(h_{\theta_+}^2 d\theta^2 + h_{\phi_+}^2 d\phi^2) = ds_+^2/\lambda_+^2$, where we used Eqs. (5) and (12). In this way, the spatial dependence of the first term of Eq. (20) becomes $\ln(ds_+/\lambda_+)$. The term $\ln ds_+$ is just the stream function for the circulating flow around the positive vortex and we discard it since the circulating flow around the vortex does not affect its motion. The remaining contribution $-\ln\lambda_+$ combines with the denominator of Eq. (20) evaluated at $\boldsymbol{r}_+$ to give the regularized local stream function on the complex plane arising from the negative vortex.[1] In addition to the usual stream function arising from the negative vortex itself, the renormalization includes a local curvature correction involving the spatial dependence of $\ln\lambda_+$.

For a more complete derivation of this local curvature correction, see Eqs. (35) and (A7) of Ref. [26]. The final result for the velocity of the positive vortex is simple:

$$\dot{\boldsymbol{r}}_+ = -\frac{\hbar}{M}\,\hat{\boldsymbol{n}}_+ \times \boldsymbol{\nabla}_+\left(\chi_{+-} + \frac{1}{2}\ln\lambda_+\right), \tag{21}$$

along with a similar expression for $\dot{\boldsymbol{r}}_-$. Here $\hat{\boldsymbol{n}}_+$ is the unit normal vector at the position $\boldsymbol{r}_+$ of the positive vortex, Eq. (12) gives the scale factor $\lambda = h_\phi/\rho$, and the stream function is

$$\chi_{+-} = \tfrac{1}{2}\ln\left(\rho_+^2 - 2\rho_+\rho_-\cos\phi_{+-} + \rho_-^2\right) = \ln\rho_{+-}, \tag{22}$$

where we introduced $\phi_{+-} = \phi_+ - \phi_-$ and the convenient abbreviation $\rho_{+-} = \sqrt{\rho_+^2 - 2\rho_+\rho_-\cos\phi_{+-} + \rho_-^2}$, which equals the distance $|z_+ - z_-|$ on the complex plane. Note that λ_+ varies throughout the complex plane, and its spatial dependence affects the dynamics of the vortex as it moves around the curved surface.

These dynamical equations are readily generalized for an overall charge-neutral set of vortices

$$\dot{\boldsymbol{r}}_j = \frac{\hbar}{M}\,\hat{\boldsymbol{n}}_j \times \boldsymbol{\nabla}_j\left(\sum_k{}' q_k\,\chi_{jk} - \frac{1}{2}q_j\,\ln\lambda_j\right), \tag{23}$$

where j runs over all vortices and the primed sum omits the single term $k = j$. Unfortunately these dynamical equations involve the local orthogonal unit vectors $\hat{\boldsymbol{\theta}}_j$ and $\hat{\boldsymbol{\phi}}_j$ which makes them less useful in practice. Instead, we recast these dynamical equations in terms of the scalar variables θ_j and ϕ_j that determine the position of the jth vortex core and the stream function χ_{jk}.

As a preliminary step, we rewrite Eq. (4) as an equation for the vector $\boldsymbol{r}(\theta,\phi)$ that defines the surface:

$$\boldsymbol{r}(\theta,\phi) = f_1(\theta)\cos\phi\,\hat{\boldsymbol{x}} + f_1(\theta)\sin\phi\,\hat{\boldsymbol{y}} + f_2(\theta)\,\hat{\boldsymbol{z}}. \tag{24}$$

Correspondingly, we have the associated unit vectors on the surface:

$$\hat{\boldsymbol{\theta}} = \frac{1}{h_\theta}\frac{\partial\boldsymbol{r}}{\partial\theta}, \quad \hat{\boldsymbol{\phi}} = \frac{1}{h_\phi}\frac{\partial\boldsymbol{r}}{\partial\phi}, \tag{25}$$

where h_θ and h_ϕ are the metric factors given in Eq. (6). In addition, the unit normal vector is

$$\hat{\boldsymbol{n}} = \hat{\boldsymbol{\theta}} \times \hat{\boldsymbol{\phi}}, \tag{26}$$

and the three vectors $(\hat{\boldsymbol{\theta}}, \hat{\boldsymbol{\phi}}, \hat{\boldsymbol{n}})$ constitute a right-handed orthonormal triad. Each of these unit vectors varies continuously around the surface.

For the jth vortex, Eqs. (24) and (25) show that

$$\dot{\boldsymbol{r}}_j = h_{\theta_j}\,\dot{\theta}_j\,\hat{\boldsymbol{\theta}}_j + h_{\phi_j}\,\dot{\phi}_j\,\hat{\boldsymbol{\phi}}_j. \tag{27}$$

The gradient vector has the familiar form

$$\boldsymbol{\nabla} = \frac{\hat{\boldsymbol{\theta}}}{h_\theta}\frac{\partial}{\partial\theta} + \frac{\hat{\boldsymbol{\phi}}}{h_\phi}\frac{\partial}{\partial\phi}. \tag{28}$$

A combination with Eq. (23) gives the desired scalar dynamical equations

$$\dot{\theta}_j = -\frac{\hbar}{M}\frac{1}{h_{\theta_j}h_{\phi_j}}\frac{\partial}{\partial\phi_j}\left(\sum_k{}' q_k\chi_{jk} - \frac{1}{2}q_j\ln\lambda_j\right), \tag{29}$$

$$\dot{\phi}_j = \frac{\hbar}{M}\frac{1}{h_{\theta_j}h_{\phi_j}}\frac{\partial}{\partial\theta_j}\left(\sum_k{}' q_k\chi_{jk} - \frac{1}{2}q_j\ln\lambda_j\right). \tag{30}$$

The last term of Eq. (29) makes no contribution because λ_j is independent of ϕ_j for any axisymmetric surface. As a result it is easy to see that

$$\sum_j q_j\,h_{\theta_j}h_{\phi_j}\,\dot{\theta}_j = -\frac{\hbar}{M}\sum_{jk}{}' q_j q_k\frac{\partial\chi_{jk}}{\partial\phi_j} = 0 \tag{31}$$

because $\partial\chi_{jk}/\partial\phi_j$ is odd under the interchange $j \leftrightarrow k$. Hence there is a conserved quantity

$$\Sigma = \sum_j q_j\sigma(\theta_j), \tag{32}$$

where $\sigma(\theta) = \int d\theta\,h_\theta h_\phi$ is an integral similar to Eq. (11) for $\ln\rho(\theta)$. Note that this conclusion $d\Sigma/dt = 0$ holds for any allowed set of quantized vortices on an axisymmetric compact surface and reflects the invariance of the surface under rotations around the z axis. In other words, the dynamics depends only on the differences ϕ_{jk}, rather than on ϕ_j and ϕ_k separately.

Equations (10) and (12) now allow us to evaluate the partial derivatives explicitly, thus expressing the dynamical

[1] In the mathematical literature, the regularized stream function is often called "the Robin function" [27].

equations wholly in terms of the coordinates of each vortex on an axisymmetric compact surface. For simplicity, we focus on a single vortex dipole, where the charge neutrality requires $q_k = -q_j$, with $j = \pm$ and $q_j = \pm 1$. A detailed calculation yields the final results

$$\dot{\theta}_j = \frac{\hbar q_j}{M h_{\theta_j} h_{\phi_j}} \frac{\rho_j \rho_k \sin\phi_{jk}}{\rho_{jk}^2}, \tag{33}$$

$$\dot{\phi}_j = -\frac{\hbar\, q_j}{2M h_{\phi_j}^2} \left(\frac{h'_{\phi_j}}{h_{\theta_j}} + \frac{\rho_j^2 - \rho_k^2}{\rho_{jk}^2} \right). \tag{34}$$

These equations have the significant advantage of being explicit coupled first-order differential equations for the dynamics of a vortex dipole on an axisymmetric compact surface. In particular, we have evaluated all relevant partial derivatives so that no variables need to be held fixed.

We now show that Eqs. (29) and (30) have a simple and direct connection with the total energy of the charge-neutral set of quantized superfluid vortices on our axisymmetric surface. In detail, we start from the total energy written in terms of the stream function χ_{kl} and the scale factor λ_k, as derived previously in Eqs. (33) and (34) of Ref. [26]:

$$E = \frac{\hbar^2 n\pi}{M} \left(-{\sum_{kl}}' q_k q_l\, \chi_{kl} + \sum_k q_k^2 \ln\lambda_k \right), \tag{35}$$

where the primed double sum omits the terms with $k = l$. This expression for the total energy is equivalent to Eq. (2.15) in Ref. [27], here expressed in physical variables χ and λ instead of mathematical ones. For a single vortex dipole with unit charges, Eq. (35) simplifies to

$$E_{\rm dipole} = \frac{\hbar^2 n\pi}{M} \ln\left(\frac{\rho_{+-}^2 \lambda_+ \lambda_-}{\xi_0^2} \right), \tag{36}$$

where we have inserted the constant core radius ξ_0 to give the renormalized vortex core $\xi_0/\lambda_\pm$ on the complex plane.

A straightforward calculation shows that the partial derivatives of E yield the desired Hamiltonian equations of motion

$$2\pi\hbar\, n\, q_j\, \dot{\theta}_j = \frac{1}{h_{\theta_j} h_{\phi_j}} \frac{\partial E}{\partial \phi_j}, \tag{37}$$

$$2\pi\hbar\, n\, q_j\, \dot{\phi}_j = -\frac{1}{h_{\theta_j} h_{\phi_j}} \frac{\partial E}{\partial \theta_j}, \tag{38}$$

with the total energy E as the effective Hamiltonian [compare Eq. (38) from Ref. [26]] and (θ_j, ϕ_j) as canonical variables.

For any Hamiltonian with no explicit time dependence, the conservation of energy follows almost by inspection. Note that

$$\frac{dE}{dt} = \sum_j \left(\frac{\partial E}{\partial \theta_j} \dot{\theta}_j + \frac{\partial E}{\partial \phi_j} \dot{\phi}_j \right). \tag{39}$$

Use of Eqs. (37) and (38) immediately shows that $dE/dt = 0$. Thus the vortex dynamics on axisymmetric compact surfaces conserves the total energy E, including the contribution of the spatially varying scale factor λ in Eq. (35) above. As noted below Eq. (32), the dynamical motion also conserves the angular momentum Σ.

IV. DESCRIPTION OF ELLIPSOIDS

Here, we specialize to an axisymmetric ellipsoid, where it is convenient to use a as length scale and write

$$ds^2 = a^2 \left(h_\theta^2\, d\theta^2 + h_\phi^2\, d\phi^2 \right). \tag{40}$$

We now have *dimensionless* metric factors

$$h_\theta = \sqrt{\cos^2\theta + (b^2/a^2)\sin^2\theta}, \quad h_\phi = \sin\theta. \tag{41}$$

Substitution of Eq. (2) into Eqs. (24)–(26) and (28) gives the detailed form of the relevant unit vectors and the gradient operator, with appropriate factors of a because of our dimensionless metric factors. For later reference, the Gaussian curvature K of an axisymmetric ellipsoid is

$$K = \frac{b^2}{\left(a^2 \cos^2\theta + b^2 \sin^2\theta \right)^2} \tag{42}$$

with the dimension of an inverse length squared.

Remarkably, there is close connection between the Gaussian curvature K and the curvature contribution $\ln\lambda$ to the energy in Eq. (35). For an isothermal metric with scale factor λ, as in Eq. (7), Brioschi's formula [32] asserts that

$$-\frac{1}{\lambda^2} \nabla^2 \ln\lambda = -\frac{1}{\lambda^2} \frac{1}{\rho} \frac{d}{d\rho} \left(\rho \frac{d\ln\lambda}{d\rho} \right) = K. \tag{43}$$

The general form on the left-hand side simplifies to the second form for the axisymmetric compact surfaces considered here, expressed in terms of the polar variables (ρ, ϕ). Brioschi's formula is effectively a nonlinear Poisson equation for $\ln\lambda$ with the Gaussian curvature K as the source.

Except for a sphere with $a = b$, the relation between the angular parameter θ and the polar (or "geocentric") angle η denoting a point on the surface of the ellipsoid is not direct, as shown in Fig. 2. For definiteness, consider an oblate ellipsoid with $a > b$ and set $\phi = 0$, namely, the right-hand side of the xz plane. Draw a circumscribed circle of radius a and an inscribed circle of radius b. Draw a straight line at angle θ from the z axis, intersecting both circles (dashed line in Fig. 2). These intersections serve to define a point P on the ellipse with $x = a\sin\theta$ and $z = b\cos\theta$. A straight line from the origin to this point P (dash-dotted line in Fig. 2) defines the "geocentric" polar angle η through the equation

$$\tan\eta \equiv \frac{x}{z} = \frac{a\sin\theta}{b\cos\theta} = \frac{a}{b}\tan\theta. \tag{44}$$

More formally, we introduce the coordinate equations [compare Eq. (2)]

$$x = L(\eta)\sin\eta\cos\phi,\ L(\eta)\sin\eta\sin\phi,\ z = L(\eta)\cos\eta. \tag{45}$$

The latter equations resemble those defining a sphere, with the important caveat that the length L now depends on η. Simple algebra with Eq. (44) shows that

$$\sin\eta = \frac{a\sin\theta}{\sqrt{a^2\sin^2\theta + b^2\cos^2\theta}},$$

$$\cos\eta = \frac{b\cos\theta}{\sqrt{a^2\sin^2\theta + b^2\cos^2\theta}}, \tag{46}$$

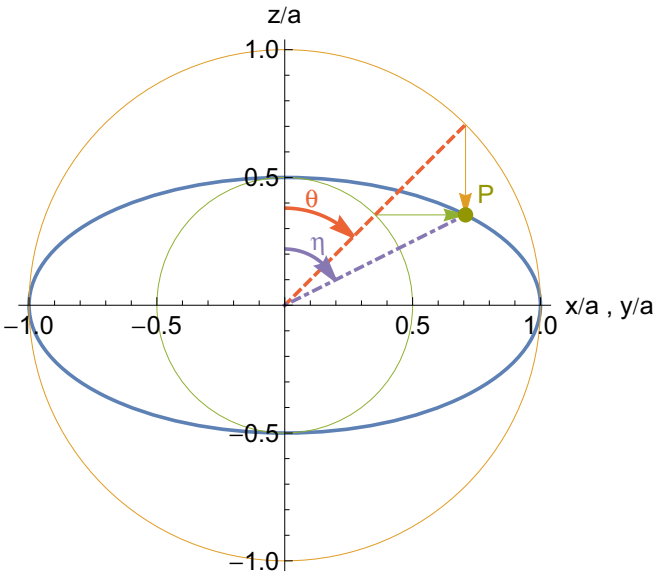

FIG. 2. Cross section of an oblate ellipsoid with $b = a/2$ along with a circumscribed circle of radius a and inscribed circle of radius b. The vertical and horizontal intersecting lines show de la Hire's construction with a dashed line at angle θ and a dash-dotted line at geocentric angle η.

with similar expressions based on the inverse relation $\tan\theta = (b/a)\tan\eta$. For a given ellipsoid and θ, these relations determine the geocentric angle η. In addition, use of Eq. (3) shows that

$$L(\eta) = \frac{ab}{\sqrt{a^2\cos^2\eta + b^2\sin^2\eta}}. \tag{47}$$

Before we specialize our general formalism from Sec. II to the surface of an axisymmetric ellipsoid, it is instructive to consider the simpler case of a sphere of radius a. In this case, Eq. (11) simplifies to

$$\rho(\theta) = \exp\left(\int^{\theta} \frac{d\tilde{\theta}}{\sin\tilde{\theta}}\right) = \tan(\theta/2) \tag{48}$$

which is precisely the standard result found with stereographic projection [5,8].

For a general ellipsoid, Eq. (11) becomes

$$\ln\rho(\theta) = \int^{\theta} d\tilde{\theta}\,\frac{\sqrt{\cos^2\tilde{\theta} + (b^2/a^2)\sin^2\tilde{\theta}}}{\sin\tilde{\theta}}, \tag{49}$$

where we use Eq. (41). The final expression depends on the details of the ellipsoid. For the oblate (disk shaped) ellipsoid with $a > b$, define the eccentricity $\epsilon_o = \sqrt{1-(b^2/a^2)}$ and

$$h_\theta = \sqrt{1-\epsilon_o^2\sin^2\theta}. \tag{50}$$

The integration in Eq. (49) gives the result for an oblate surface:

$$\rho_o(\theta) = \frac{h_\theta - \cos\theta}{\sin\theta}\,(h_\theta + \epsilon_o\cos\theta)^{\epsilon_o}. \tag{51}$$

For the prolate (cigar shaped) ellipsoid with $b > a$, the parameter ϵ_o becomes imaginary. We define $\zeta = i\epsilon_o$ with the real quantity $\zeta = \sqrt{(b^2/a^2)-1}$, giving

$$h_\theta = \sqrt{1+\zeta^2\sin^2\theta}. \tag{52}$$

The final answer for a prolate surface follows from Eq. (49):

$$\rho_p(\theta) = \frac{h_\theta - \cos\theta}{\sin\theta}\,\exp\left[-\zeta\,\arcsin\left(\frac{\zeta\cos\theta}{\sqrt{1+\zeta^2}}\right)\right]. \tag{53}$$

To interpret this result, we note that a prolate ellipsoid has the eccentricity $\epsilon_p = \sqrt{1-(a^2/b^2)} = \zeta/\sqrt{1+\zeta^2}$. Equivalently, we have $\zeta = \epsilon_p/\sqrt{1-\epsilon_p^2}$. Some algebra shows that Eq. (53) has the equivalent form

$$\rho_p(\theta) = \frac{\sqrt{1-\epsilon_p^2\cos^2\theta} - \sqrt{1-\epsilon_p^2}\cos\theta}{\sin\theta} \times \exp\left[-\frac{\epsilon_p}{\sqrt{1-\epsilon_p^2}}\arcsin(\epsilon_p\cos\theta)\right], \tag{54}$$

where we omit an overall constant factor in the denominator that does not affect the dynamics of the vortices.

V. VORTEX DYNAMICS ON AN ELLIPSOID

We now apply the results from Sec. III to study the dynamics of a vortex dipole with unit charges $q_\pm = \pm 1$ on an axisymmetric ellipsoid, with the metric given by Eqs. (40) and (41). Equation (33) yields

$$h_{\theta_+}\sin\theta_+\dot{\theta}_+ = h_{\theta_-}\sin\theta_-\dot{\theta}_- = \frac{\hbar}{Ma^2}\,\frac{\rho_+\rho_-\sin\phi_{+-}}{\rho_{+-}^2}. \tag{55}$$

In addition, Eq. (34) gives

$$\dot{\phi}_+ = -\frac{\hbar}{2Ma^2\sin^2\theta_+}\left(\frac{\cos\theta_+}{h_{\theta_+}} + \frac{\rho_+^2-\rho_-^2}{\rho_{+-}^2}\right) \tag{56}$$

with a similar equation for $\dot{\phi}_-$. As noted below Eqs. (33) and (34), these equations are explicit first-order ordinary differential equations for the dynamics of a vortex dipole on an axisymmetric ellipsoid. Finally the total energy in Eq. (35) for such a dipole reduces to

$$E = \frac{\hbar^2 n\pi}{M}\ln\left(\rho_{+-}^2\lambda_+\lambda_-\right), \tag{57}$$

which shows the joint role of the stream function (through the first factor) and the scale factors $\lambda_\pm$.

A. Special case of a sphere

A sphere has $a = b$ so that $h_\theta = 1$. Correspondingly, the radial distance on the complex plane becomes [compare Eq. (48)]

$$\rho(\theta) = \tan\left(\frac{\theta}{2}\right) = \frac{\sin\theta}{1+\cos\theta} = \sqrt{\frac{1-\cos\theta}{1+\cos\theta}}. \tag{58}$$

The scale factor in Eq. (12) simplifies to

$$\lambda(\theta) = \frac{\sin\theta}{\rho(\theta)} = 1+\cos\theta, \tag{59}$$

which depends on θ even though a sphere has constant Gaussian curvature.

For a sphere, it is not difficult to show that [8]

$$\rho_{+-}^2 = \frac{4\sin^2(\gamma_{+-}/2)}{\lambda_+\lambda_-}, \tag{60}$$

where γ_{+-} is the angle between $\hat{\boldsymbol{r}}_+$ and $\hat{\boldsymbol{r}}_-$. As a result, the scale factors in Eq. (57) cancel exactly, and the energy of a vortex dipole on a sphere has the very simple form [see Eq. (57)]

$$E_{\rm dipole} = \frac{2\hbar^2 n\pi}{M}\ln\left[2\sin(|\gamma_{+-}|/2)\right]. \tag{61}$$

Although the scale factors cancel for the special case of a sphere, the terms $\ln\lambda_\pm$ generally play a role in the energy and the dynamics of a vortex dipole on an axisymmetric compact surface.

Note that $2a\sin(|\gamma_{+-}|/2)$ is the chordal distance between the two members of the vortex dipole [5,8]. Hence the dynamical motion of any dipole on a sphere conserves the chordal distance between them. When the radius a of the sphere is much larger than the separation r of the dipole, the angular aperture becomes small with $\gamma_{+-} \ll 1$. In this limit, the chordal length approaches the usual planar length, and Eq. (61) reduces to the well-known flat case proportional to $\ln(r/\xi_0)$, apart from an additive constant $\ln(a/\xi_0)$.

The high symmetry of a sphere allows us to consider (without loss of generality) a symmetric initial configuration relative to the equator, with $\theta_+ = \theta$ and $\theta_- = \pi - \theta$ and $\phi_{+-} = 0$. Equation (48) shows that $\rho_\pm = (1 \mp \cos\theta)/\sin\theta$. In this symmetric configuration, some algebra with Eqs. (55) and (56) gives the familiar result [5]

$$\dot{\boldsymbol{r}}_+ = \dot{\boldsymbol{r}}_- = \frac{\hbar\hat{\boldsymbol{\phi}}}{2Ma}\tan\theta, \tag{62}$$

so that the vortex dipole moves uniformly in the common $\hat{\boldsymbol{\phi}}$ direction along the great circle midway between them (the equator). The vortices become stationary in the limit $\theta \to 0$, when they approach the north and south poles. Near the equator, when $\theta \to \pi/2 - \delta\theta$, the translational velocity diverges, with $\dot{\boldsymbol{r}}_+ = \dot{\boldsymbol{r}}_- = \hbar\hat{\boldsymbol{\phi}}/(2Ma\,\delta\theta)$, which is just the result for a vortex dipole on a plane since $2a\,\delta\theta$ is their spatial separation.

B. Dipole placed symmetrically around the equator

As a first example of a vortex dipole on an axisymmetric ellipsoid, we consider the special configuration with the dipole symmetrically placed on either side of the equator, with $\theta_+ = \theta, \theta_- = \pi - \theta$, and $\phi_{+-} = 0$. Here, the motion is purely azimuthal with

$$\dot{\boldsymbol{r}}_+ = \dot{\boldsymbol{r}}_- = -\frac{\hbar\hat{\boldsymbol{\phi}}}{2Ma\sin\theta}\left(\frac{\cos\theta}{h_\theta} + \frac{\rho_+ + \rho_-}{\rho_+ - \rho_-}\right), \tag{63}$$

where

$$\rho_\pm = \frac{h_\theta \mp \cos\theta}{\sin\theta}\,\delta_\pm. \tag{64}$$

Here,

$$\delta_\pm = (h_\theta \pm \epsilon_o\cos\theta)^{\epsilon_o} \tag{65}$$

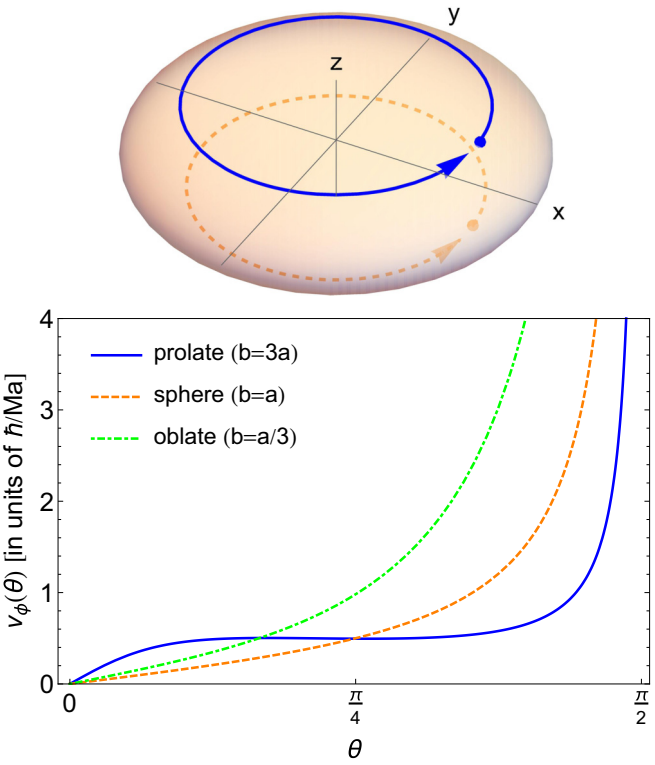

FIG. 3. Upper panel: Circulating orbits of positive (solid blue) and negative (dashed orange) members of a vortex dipole placed symmetrically above and below the equator. Lower panel: Translational velocity of a vortex dipole symmetrically placed around the equator for prolate and oblate ellipsoids with aspect ratios $b/a = 3$ ($\epsilon_p = 2\sqrt{2}/3 \approx 0.943$) and $a/b = 3$ ($\epsilon_o = 2\sqrt{2}/3 \approx 0.943$).

for an oblate ellipsoid with eccentricity ϵ_o, and

$$\delta_\pm = \exp\left[\mp\frac{\epsilon_p}{\sqrt{1-\epsilon_p^2}}\arcsin(\epsilon_p\cos\theta)\right]$$
$$= \exp\left[\mp\zeta\arcsin\left(\frac{\zeta\cos\theta}{\sqrt{1+\zeta^2}}\right)\right] \tag{66}$$

for a prolate ellipsoid with eccentricity ϵ_p. For either distortion, it is not difficult to show that

$$\dot{\boldsymbol{r}}_+ = \dot{\boldsymbol{r}}_- = \frac{\hbar b^2\hat{\boldsymbol{\phi}}}{2Ma^3 h_\theta}\frac{\sin\theta(\delta_+ + \delta_-)}{\cos\theta(\delta_+ + \delta_-) - h_\theta(\delta_+ - \delta_-)}. \tag{67}$$

Since $\delta_+ - \delta_-$ vanishes for a sphere, this expression reduces to Eq. (62) in the spherical limit.

Figure 3 shows the orbits and azimuthal translational speed $v_\phi(\theta)$ of a vortex dipole symmetrically placed around the equator for a sphere and for oblate and prolate ellipsoids with $a/b = 3$ and $1/3$, respectively ($\epsilon_o = \epsilon_p = 2\sqrt{2}/3 \approx 0.943$). The orbits themselves are independent of the aspect ratio, but the lower panel in Fig. 3 shows how the speed of the dipole varies with polar angle θ.

The energy of a vortex dipole on an elongated surface depends linearly on the separation $d = |\boldsymbol{r}_+ - \boldsymbol{r}_-|$ once d exceeds the radial dimension [10,31,33], instead of the usual logarithmic dependence when d is small. For an ellipsoid, the translational velocity $\dot{\boldsymbol{r}}_+$ is proportional to $\hat{\boldsymbol{n}}_+ \times \boldsymbol{\nabla}_+ E$, and

the linear dependence of the energy on d thus explains the extended flat region for a prolate ellipsoid when $d \gtrsim a$. In fact, the translational speed for a vortex dipole with $d \gtrsim R$ on an infinite cylinder with radius R is $\hbar/(2MR)$ [10]. The curve labeled *prolate* in the lower panel of Fig. 3 shows that the numerical value for our prolate ellipsoid agrees closely with the result for an infinite cylinder of radius $R = b/3$.

C. Energy considerations

The above discussion of the dynamics of a special vortex dipole simplifies greatly because both vortices execute purely azimuthal motion along the common direction $\hat{\boldsymbol{\phi}}$. Other initial configurations typically involve different unit vectors, and it is generally easier to start from the total energy $E_{\rm tot}$ in Eq. (35).

The simplest vortex configuration on a compact surface is a vortex dipole with unit charges. For this case, a combination of $\lambda_\pm = \sin\theta_\pm/\rho_\pm$ and Eq. (57) shows that the dipole energy becomes

$$E_{\rm dipole} = \frac{\hbar^2 n\pi}{M} \ln Q, \tag{68}$$

with the conserved quantity Q for a vortex dipole on an ellipsoid:

$$Q = \left(\frac{\rho_+}{\rho_-} - 2\cos\phi_{+-} + \frac{\rho_-}{\rho_+}\right) \sin\theta_+ \sin\theta_-. \tag{69}$$

This expression Q has several desirable features.

(1) Q is manifestly symmetric under interchange of vortices $(\theta_+, \phi_+) \leftrightarrow (\theta_-, \phi_-)$.

(2) It depends only on the combination $\phi_{+-} = \phi_+ - \phi_-$ reflecting the axisymmetry of the surface.

(3) As noted in Sec. IV, the integration for $\ln\rho$ leads to an arbitrary additive constant, and hence an arbitrary multiplicative constant for ρ. Equation (69) shows that this constant cancels in the conserved quantity Q.

Although Hamilton's equations are elegant, in any particular case they involve partial derivatives with other variables held fixed. Hence it is frequently simpler to rely on Eqs. (55) and (56) that depend explicitly on the local positions, as seen in the following Sec. V D.

D. Vortex dipole moving north from the equator

We now consider the special initial configuration of a vortex dipole with $\theta_+ = \theta_- = \theta$, starting at the equator with $\theta_0 = \pi/2$. This symmetry ensures that $\theta_+ = \theta_-$ and therefore $\rho_+ = \rho_-$ for all later times. In addition, we choose the initial value for $(\phi_- - \phi_+)_0 = \Delta_0$ to be in the range $0 < \Delta_0 < \pi$, so that the vortex dipole starts moving toward the north pole. The energy for this vortex configuration has a particularly simple form

$$E = \frac{\hbar^2 n\pi}{M} \ln\left[4\sin^2\theta \sin^2\left(\frac{\Delta}{2}\right)\right], \tag{70}$$

so that

$$Q = 4\sin^2\theta \sin^2(\Delta/2) \tag{71}$$

from Eq. (69).

For these initial conditions, $\sin\theta$ decreases from 1 and $\sin(\Delta/2)$ increases from $\sin(\Delta_0/2)$. Eventually $\sin(\Delta/2)$ reaches its maximum value 1 for $\Delta = \pi$ as the vortex dipole moves over the shoulder at the polar angle $\theta_{\rm min} = \Delta_0/2$. The vortex dipole then moves back toward the equator on the opposite side of the ellipsoid, with Δ now decreasing and $\sin\theta$ correspondingly increasing. Evidently, this motion will repeat cyclically, as seen in Fig. 4.

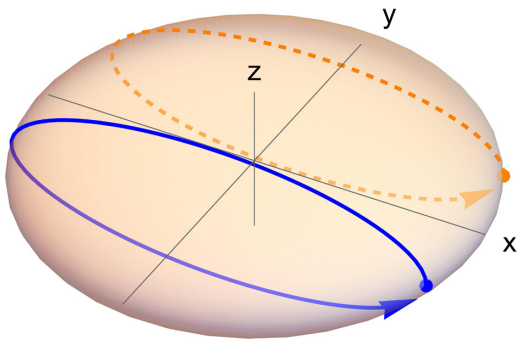

FIG. 4. Circulating orbits of positive (solid blue) and negative (dashed orange) members of a vortex dipole, starting from the equator $\theta = \pi/2$, marked by dots.

How does this Q compare with the squared chordal distance? In this specific highly symmetric case it is easy to verify that $|\boldsymbol{r}_+ - \boldsymbol{r}_-|^2 = r_{+-}^2 = 4a^2\sin^2\theta\sin^2(\Delta/2) = a^2 Q$, so that the dynamical motion indeed conserves the chordal distance. As seen below, more generic initial configurations of the vortex dipole will not conserve the chordal distance.

It is instructive to write out the corresponding dynamical equation for the angular variables. Equations (55) and (56) together give

$$\dot\theta_- = \dot\theta_+ = -\frac{\hbar}{2Ma^2 h_\theta \sin\theta} \cot(\Delta/2), \tag{72}$$

$$\dot\phi_- = -\dot\phi_+ = \frac{\hbar}{2Ma^2 h_\theta \sin\theta} \cot\theta. \tag{73}$$

As expected from the conservation of Q, we see that the two polar angles move together while the two azimuthal angles move to conserve their sum.

E. General asymmetric case

If the initial locations of the two vortices do not obey special symmetries, the ensuing dynamics becomes much more complex. One such example is shown in Fig. 5. The two vortices perform a relatively regular motion, but their orbits are not closed.

We checked in detail that the dynamical motion conserves both the total energy E and the "angular momentum" Σ defined in Eq. (32). The upper image of Fig. 6 shows that the chordal distance is definitely not constant, unlike our previous examples. Instead, it oscillates anharmonically but nonetheless periodically. The middle image shows that the speed of each vortex also varies periodically but at half the frequency of the chordal distance. In contrast, the sum of the squared speeds of the two vortices $|\dot{\boldsymbol{r}}_1|^2 + |\dot{\boldsymbol{r}}_2|^2$ oscillates exactly in phase with (and with the same period of) the chordal distance. Here the squared speed is given by $|\dot{\boldsymbol{r}}|^2 = a^2 h_\theta^2 \dot\theta^2 + a^2 h_\phi^2 \dot\phi^2$. The lower panel shows the local Gaussian curvature at the

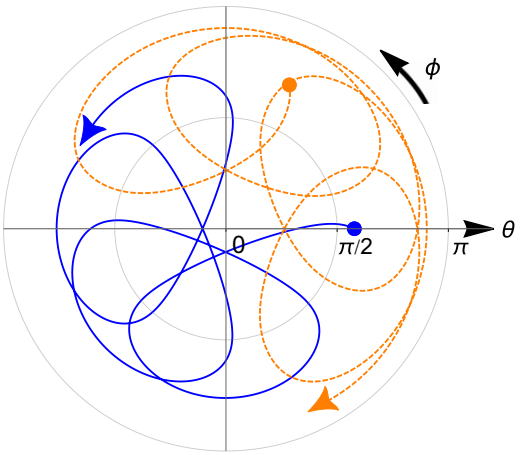

FIG. 5. Circulating orbits of positive (solid blue) and negative (dashed orange) members of a vortex dipole, starting from two arbitrary points (marked by dots), for an oblate ellipsoid with aspect ratio $b/a = 1/3$ ($\epsilon_o \approx 0.943$). The vortices execute a quasiperiodic motion without forming closed orbits. See the Supplemental Material [34] for a video displaying the simulation of this dynamics.

position of each vortex:

$$K = \frac{1-\epsilon_o^2}{a^2(1-\epsilon_o^2\sin^2\theta)^2}, \tag{74}$$

here written for an oblate ellipsoid. Comparison of the middle and lower panels of Fig. 6 highlights the anticorrelation between the vortex speed and the local curvature of the surface: vortices slow down in the regions of higher curvature.

VI. CONCLUSIONS

We have constructed a theory of quantized superfluid two-dimensional vortices on axisymmetric compact surfaces with no holes. Specifically, we developed a general method to transform conformally from the axisymmetric surface to a plane, where we use familiar methods based on the hydrodynamic stream function. This transformation yields an additional term in the dynamics of each vortex reflecting the local curvature at its position. Our approach shows the close connection to the energy of these vortices. They constitute a Hamiltonian dynamical system, with the angular positions (θ_j, ϕ_j) as canonical variables.

A vortex dipole is the simplest superfluid state that satisfies the condition of vanishing total vortex charge. We study the dynamics of two simple symmetric vortex-dipole configurations and then consider a more general asymmetric initial configuration, showing trajectories and other related quantities. Unlike the situation on a sphere, the chordal distance is not in general a constant of the motion.

In recent years, various mathematicians have studied two-dimensional vortices on axisymmetric surfaces [27–29] and triaxial ellipsoids [30]. In particular, Ref. [27] independently developed the same method for vortices on axisymmetric surfaces based on conformal mapping. All their examples treat classical vortices, frequently focusing on large-scale atmospheric vortices and polygonal rings of identical vortices. In these examples, one or more polar vortices (or sometimes uniform vorticity) enforce the condition of net vortex-charge neutrality. Another example of mathematical interest is the classical three-vortex problem on a sphere [35], where at least two of them necessarily have different absolute vortex charges.

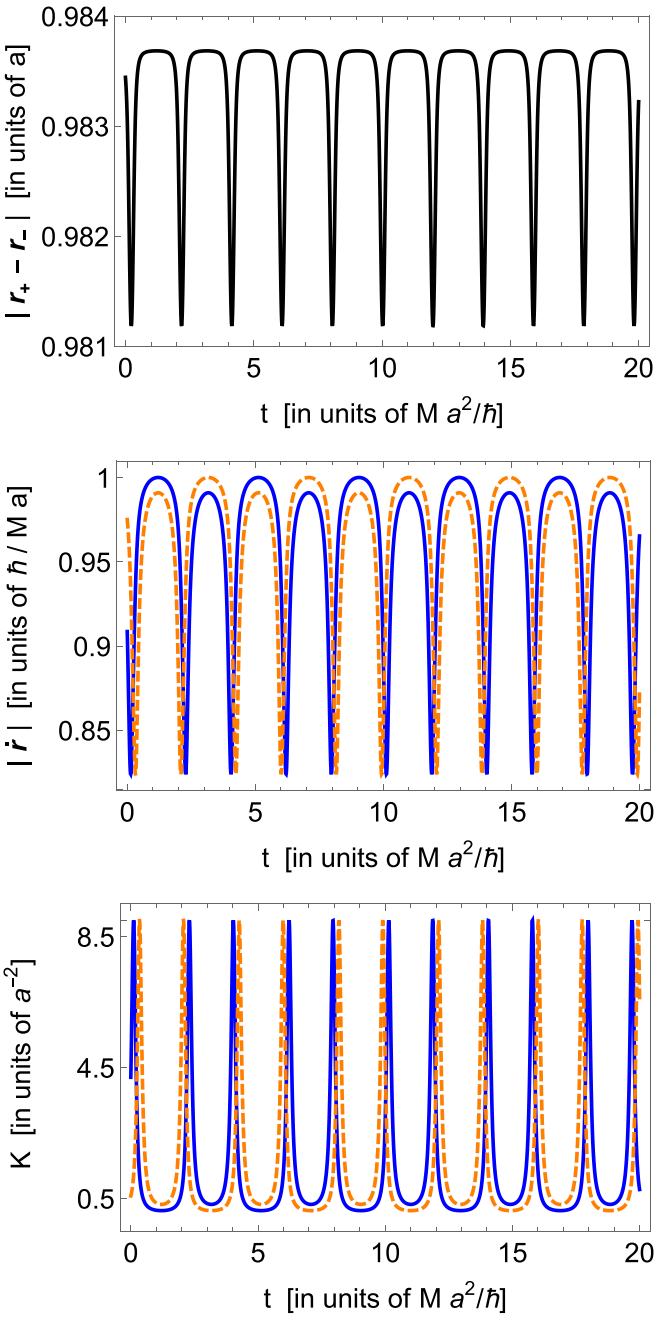

FIG. 6. Upper panel: Time evolution of chordal distance. Middle panel: Speed of positive (solid blue) and negative (dashed orange) vortices. Lower panel: Local Gaussian curvature for the positive (solid blue) and negative (dashed orange) vortices for the particular asymmetric configuration represented in Fig. 5.

The situation is quite different for the quantized superfluid vortices that we study here. Typically all the vortices have unit charge ($q_j = \pm 1$) and the condition of irrotational flow precludes distributed vorticity. The simplest superfluid configuration is a vortex dipole, and we studied several examples of vortex dynamics on an ellipsoid.

Reference [26] studied superfluid vortex dynamics on a torus and other toroids of revolution, extending Kirchhoff's conformal transformation from a torus to a plane [25]. It would be interesting to study more general multiply connected surfaces (such as a pretzel) with two or more holes, where each nontrivial quantized circulation loop will contribute to the vortex dynamics. In such cases, however, the absence of rotational invariance presents a definite challenge.

Most studies of vortex dynamics on curved superfluid films assume a uniform thickness and density. In practice, experiments on Earth have to deal with the presence of gravity, which significantly alters the distribution of atoms along the shell's surface [36,37]. Recent observations with the NASA Cold Atom Laboratory [22] (see also the theoretical analysis in Ref. [38]) suggest that asymmetries in the apparatus will produce films with nonuniform number density. The method of a time-dependent variational Lagrangian has been successful for dynamical studies of nonuniform three-dimensional Bose-Einstein condensates [39], and a similar approach should be useful for nonuniform films.

A recent study has shown that a two-component BEC can support vortices with filled cores. The resulting composite structure acts like a massive vortex and obeys second-order differential equations, very different from the usual first-order equation of vortex dynamics. For example, the familiar precession of a one-component vortex in a trap can also include small-amplitude rapid oscillations around the uniform motion [40]. It would be interesting to extend these studies to a vortex dipole on a sphere and other axisymmetric surfaces.

ACKNOWLEDGMENTS

M.A.C. acknowledges support by the São Paulo Research Foundation under Grant No. 2013/07276-1. P.M. acknowledges support by Grant No. PID2020-113565GB-C21 funded by MCIN/AEI/10.13039/501100011033, by the European Union FEDER Quantumcat, and by the US National Science Foundation under Grant No. NSF PHY-1748958.

[1] R. J. Donnelly, *Quantized Vortices in Helium II* (Cambridge University, Cambridge, England, 1991).
[2] C. Pethick and H. Smith, *Bose-Einstein Condensation in Dilute Gases*, 2nd ed. (Cambridge University, Cambridge, England, 2008).
[3] L. Pitaevskii and S. Stringari, *Bose-Einstein Condensation and Superfluidity*, 2nd ed. (Oxford University, New York, 2016).
[4] G. R. Kirchhoff, *Vorlesungen über Mathematische Physik, Bd. 1: Mechanik* (Teubner, Leipzig, 1876).
[5] H. Lamb, *Hydrodynamics*, 6th ed. (Dover, New York, 1945).
[6] L. Onsager, Nuovo Cim. **6 (Suppl.)**, 249 (1949).
[7] R. P. Feynman, Application of Quantum Mechanics to Liquid Helium, Prog. Low Temp. Phys. **1**, 17 (1955).
[8] S. J. Bereta, M. A. Caracanhas, and A. L. Fetter, Superfluid vortex dynamics on a spherical film, Phys. Rev. A **103**, 053306 (2021).
[9] T.-L. Ho and B. Huang, Spinor Condensates on a Cylindrical Surface in Synthetic Gauge Fields, Phys. Rev. Lett. **115**, 155304 (2015).
[10] N.-E. Guenther, P. Massignan, and A. L. Fetter, Quantized superfluid vortex dynamics on cylindrical surfaces and planar annuli, Phys. Rev. A **96**, 063608 (2017).
[11] P. Massignan and A. L. Fetter, Superfluid vortex dynamics on planar sectors and cones, Phys. Rev. A **99**, 063602 (2019).
[12] K. Sun, K. Padavić, F. Yang, S. Vishveshwara, and C. Lannert, Static and dynamic properties of shell-shaped condensates, Phys. Rev. A **98**, 013609 (2018).
[13] J. Zhang and T.-L. Ho, Potential scattering on a spherical surface, J. Phys. B **51**, 115301 (2018).
[14] S. Bereta, L. Madeira, V. Bagnato, and M. Caracanhas, Bose-Einstein condensation in spherically symmetric traps, Am. J. Phys. **87**, 924 (2019).
[15] A. Tononi and L. Salasnich, Bose-Einstein Condensation on the Surface of a Sphere, Phys. Rev. Lett. **123**, 160403 (2019).
[16] A. Tononi, A. Pelster, and L. Salasnich, Topological superfluid transition in bubble-trapped condensates, arXiv:2104.04585 (2021).
[17] Y. P. Sachkou, C. G. Baker, G. I. Harris, O. R. Stockdale, S. Forstner, M. T. Reeves, X. He, D. L. McAuslan, A. S. Bradley, M. J. Davis, and W. P. Bowen, Coherent vortex dynamics in a strongly interacting superfluid on a silicon chip, Science **366**, 1480 (2019).
[18] Y. Colombe, E. Knyazchyan, O. Morizot, B. Mercier, V. Lorent, and H. Perrin, Ultracold atoms confined in rf-induced two-dimensional trapping potentials, Europhys. Lett. **67**, 593 (2004).
[19] B. M. Garraway and H. Perrin, Recent developments in trapping and manipulation of atoms with adiabatic potentials, J. Phys. B **49**, 172001 (2016).
[20] N. Lundblad, R. A. Carollo, C. Lannert, M. J. Gold, X. Jiang, D. Paseltiner, N. Sergay, and D. C. Aveline, Shell potentials for microgravity Bose-Einstein condensates, npj Microgravity **5**, 30 (2019).
[21] D. C. Aveline, J. R. Williams, E. R. Elliott, C. Dutenhoffer, J. R. Kellogg, J. M. Kohel, N. E. Lay, K. Oudrhiri, R. F. Shotwell, N. Yu, and R. J. Thompson, Observation of Bose–Einstein condensates in an Earth-orbiting research lab, Nature (London) **582**, 193 (2020).
[22] R. Carollo, D. Aveline, B. Rhyno, S. Vishveshwara, C. Lannert, J. Murphree, E. Elliott, J. Williams, R. Thompson, and N. Lundblad, Observation of ultracold atomic bubbles in orbital microgravity, arXiv:2108.05880 (2021).
[23] D. V. Freilich, D. M. Bianchi, A. M. Kaufman, T. K. Langin, and D. S. Hall, Real-Time Dynamics of Single Vortex Lines and Vortex Dipoles in a Bose-Einstein Condensate, Science **329**, 1182 (2010).
[24] K. Padavić, K. Sun, C. Lannert, and S. Vishveshwara, Vortex-antivortex physics in shell-shaped Bose-Einstein condensates, Phys. Rev. A **102**, 043305 (2020).

[25] G. Kirchhoff, Über die stationären elektrischen Strömungen in einer gekrümmten leitenden Fläche, Monatsber. Akad. Wiss. Berlin **19**, 487 (1875).

[26] N.-E. Guenther, P. Massignan, and A. L. Fetter, Superfluid vortex dynamics on a torus and other toroidal surfaces of revolution, Phys. Rev. A **101**, 053606 (2020).

[27] D. G. Dritschel and S. Boatto, The motion of point vortices on closed surfaces, Proc. R. Soc. A **471**, 20140890 (2015).

[28] D. Hally, Stability of streets of vortices on surfaces of revolution with a reflection symmetry, J. Math. Phys. **21**, 211 (1980).

[29] C. Castilho and H. Machado, The N-vortex problem on a symmetric ellipsoid: A perturbation approach, J. Math. Phys. **49**, 022703 (2008).

[30] A. Regis Rodrigues, C. Castilho, and J. Koiller, Vortex pairs on a triaxial ellipsoid and Kimura's conjecture, J. Geom. Mech. **10**, 189 (2018).

[31] A. M. Turner, V. Vitelli, and D. R. Nelson, Vortices on curved surfaces, Rev. Mod. Phys. **82**, 1301 (2010).

[32] A. Gray, *Modern Differential Geometry of Curves and Surfaces* (CRC, Boca Raton, FL, 1993).

[33] J. Machta and R. A. Guyer, Superfluid films on a cylindrical surface, J. Low Temp. Phys. **74**, 231 (1989).

[34] See Supplemental Material at http://link.aps.org/supplemental/10.1103/PhysRevA.105.023307 for a video of the dynamics of a superfluid vortex dipole on the surface of an ellipsoid, as given by Fig. 5.

[35] P. Newton, *The N-Vortex Problem* (Springer, New York, 2001).

[36] K. Merloti, R. Dubessy, L. Longchambon, A. Perrin, P.-E. Pottie, V. Lorent, and H. Perrin, A two-dimensional quantum gas in a magnetic trap, New J. Phys. **15**, 033007 (2013).

[37] Y. Guo, E. M. Gutierrez, D. Rey, T. Badr, A. Perrin, L. Longchambon, V. Bagnato, H. Perrin, and R. Dubessy, An annular quantum gas induced by dimensional reduction on a shell, arXiv:2105.12981 (2021).

[38] A. Tononi, F. Cinti, and L. Salasnich, Quantum Bubbles in Microgravity, Phys. Rev. Lett. **125**, 010402 (2020).

[39] V. M. Pérez-García, H. Michinel, J. I. Cirac, M. Lewenstein, and P. Zoller, Low Energy Excitations of a Bose-Einstein Condensate: A Time-Dependent Variational Analysis, Phys. Rev. Lett. **77**, 5320 (1996).

[40] A. Richaud, V. Penna, and A. L. Fetter, Dynamics of massive point vortices in a binary mixture of Bose-Einstein condensates, Phys. Rev. A **103**, 023311 (2021).